High Conductivity Copper-Carbon Nanotube Hybrids via Site-Specific Chemical Vapor Deposition

*Anthony P. Leggiero[a,b]; Kylie J. Trettner[b,c]; Heather L. Ursino[b,c]; Dylan J. McIntyre[a,b]; Mark Schauer[d]; Eitan Zeira[d]; Cory D. Cress[e]; Brian J. Landi[b,c]**

a) Department of Microsystems Engineering, Rochester Institute of Technology, Rochester, New York 14623, United States

b) NanoPower Research Laboratories, Rochester Institute of Technology, Rochester, New York 14623, United States

c) Department of Chemical Engineering, Rochester Institute of Technology, Rochester, New York 14623, United States

d) Nanocomp Technologies, Inc., Merrimack, New Hampshire 03054, United States

e) Electronics Science and Technology Division, United States Naval Research Laboratory, Washington, District of Columbia 20375, United States

KEYWORDS

Carbon nanotube; composite conductors; hybrid conductors; chemical vapor deposition; $Cu(tBAOAC)_2$; Cu-CNT; NICCs

ABSTRACT

In this study, site-selective copper nanometal seeding through chemical vapor deposition (CVD) is demonstrated as a viable method in concert with solution electrodeposition of bulk Cu to enhance the electrical conductivity of a porous, low-density (0.12 g/cm^3, ~9 mg/m) CNT roving. An electrical bias applied directly to the CNT roving promotes Joule heating which provides the thermal energy necessary for the decomposition of a bis(t-butylacetoacetato) copper ($Cu(tBAOAC)_2$) precursor. Localized changes in the resistance within the bulk CNT conductor were used to selectively deposit the precursor at thermally active sites, which were evaluated through thermal imaging. The deposition varies from localized Cu deposits at currents producing average temperatures of ~225°C to a consistent deposition of 10-40 nm Cu particles at applied currents producing average temperatures >300°C, far above the threshold for the decomposition of the $Cu(tBAOAC)_2$ precursor. Scanning electron microscopy of a cross-section of the roving reveals Cu depositions on the interior of the roving, demonstrating the penetration of the vapor into the CNT network and subsequent decomposition within the roving. A commercial acid-based Cu electroplating solution was used to deposit bulk Cu onto as-prepared and CVD seeded CNT wires, followed by planar densification and H_2/Ar annealing. The finished conductors with Cu loadings from ~30-95% w/w which combine CVD Cu seeding and electrodeposition result in specific conductivity values 3-5X higher than Cu-CNT conductors produced by electrodeposition alone. Ultimately, a CNT hybrid conductor with 94.2% w/w Cu, achieved a specific conductivity

of 5632 S m^2/kg and electrical conductivity of 28.1 MS/m; approaching values previously only seen in metallic conductors. Overall, the present results demonstrate the potential of site-specific CVD towards both seeding metal prior to electroplating and as a possible method towards the enhanced nanometal interconnection of carbon conductors (NICCs).

TEXT

Introduction

Carbon nanotubes (CNTs) exhibit great promise for electrical conductor applications due to a combination of high electrical conductivity,[1] great flexure tolerance,[2] high tensile strength,[3] and an order of magnitude lower temperature coefficient of resistance relative to conventional wiring metals.[4,5] Individual carbon nanotubes have exhibited conductivities as high as 10^8 S/m, [2] higher even than that of traditional metallic conductors such as copper (with a conductivity of 5.8 x 10^7 S/m).[6] However, the junctions between individual carbon nanotubes[7] and bundles of CNTs,[8] along with their alignment within the bulk structure[9] presents a unique challenge in the translation of the electrical conductivity to bulk structures. Over the past few decades much research has been done toward improving the characteristics of bulk conductors.[2,10] Some methods have focused on fabrication of the CNT conductors themselves, with a focus on limiting the amount of empty space and resistive junctions in as-produced wires.[1,11,12] While other post-processing techniques such as stretching,[13] ionic doping,[14–16] densifications,[17–19] and heat treatments[20] have also been employed to lower the resistance within the micro- and nanostructure of a CNT wire. This has led to chemically doped CNT wires with conductivities approaching 10^7 S/m.[12] Alternatively, efforts are also focused on combining CNTs with traditional metallic conductors to produce hybrids which aim to combine the advantages of each material into one combined conductor.[21–26]

Recent efforts to produce metal-CNT hybrid conductors have typically focused on electrodeposition[21–24] or physical vapor deposition[25–27] methods. While high-quality coatings can be produced through either of these methods, they share a disadvantage in that the depositions are not intentionally site-specific. Instead, the deposited metal results at all locations across the CNT surface and/or within the CNT network. Furthermore, penetrating techniques such as organic electroplating can often take a full 24 hours to deposit an appropriate amount of copper seeds for further processing (e.g. through aqueous electrodeposition).[28] In addition, some studies[24,26] have observed that, in certain configurations, layered structures of copper deposited onto CNTs produce higher conductivity than structures with partially intermixed copper and CNTs. In such studies[24] the partial intermixing of copper and CNTs leads to a large number of discretized copper islands that provide negligible contributions to the conductivity of the resultant wire, resulting in wasted mass. Alternatively, if a method could deposit copper throughout the CNT network, specifically targeting areas of higher resistance, it could greatly improve the utilization of deposited copper mass by allowing for the presence of additional copper where it is needed.

In nanoscale studies, it has been demonstrated that the Joule heating of junctions between individual carbon nanotubes may be used to drive the deposition of metal from a gaseous organometallic precursor.[29] The deposited metal bridges the CNT junctions, improving the electrical conductivity of the network. Applications of this principle towards bulk CNT wires have yet to be explored. Ideally, by preferentially depositing metal at the higher temperature junctions within a bulk CNT wire, the amount of surplus non-contributing metal can be limited, thereby improving the utilization of metal mass and volume within the conductor.

In the present study, the combination of a one-hour, permeating chemical vapor deposition (CVD) technique followed by conventional electroplating is explored. In the first step, a Joule-heated carbon nanotube conductor is exposed to a Bis(t-butylacetoacetato) copper(II) ($Cu(tBAOAC)_2$) CVD precursor. The higher temperature regions in the conductor cause the preferential decomposition of the copper-containing organometallic precursor to deposit nanoscale copper seeds, representing a "continuous filament heating CVD" (CFH-CVD) approach. This $Cu(tBAOAC)_2$ precursor was chosen due to its relatively low decomposition temperature and propensity for depositing small particles,[30] which is ideal for targeting junctions within the CNT network. Thermal imaging is utilized to evaluate the heating of the roving towards the determination of proper temperature for deposition to occur. An electrodeposition step is employed to provide a cohesive overcoat, connecting the various areas of preferentially deposited copper seeds within the sample. The electrical properties (specific conductivity[1,2,10] and conductivity) of the Cu-CNT hybrid conductors are measured and compared to the literature on the basis of efficient metal utilization.

Results and Discussion

The chemical vapor deposition setup was assembled using a three-neck flask for the site-specific deposition of nanometal onto the CNT conductor. This setup is outlined in Figure 1a. The conductor chosen was an unspun CNT roving material from Nanocomp Technologies Inc., an image of which is presented at the top of Figure 1b. The CNT roving material was chosen due to its high porosity, which allows for greater penetration by the CVD precursor. The CNT roving is connected between two copper clips acting as electrical leads and suspended across the center of the flask above the CVD precursor. The $Cu(tBAOAC)_2$ precursor is heated to a vapor by a mantle at the bottom of the flask. An electrical bias applied to the CNT roving promotes current

flow which induces Joule heating, providing the thermal energy necessary to locally decompose the vapor precursor for deposition. The attachment of the flask to a Schlenk line allows for control over the local deposition environment within the flask, allowing for the application of vacuum or a reducing gas (5 mol% H_2/95 mol% Ar).

Initial tests were carried out to measure the effect of applied current on the CNT roving temperature. An electrical bias was applied to the roving in air, and temperature measurements were determined with a FLIR A35 thermal camera, corrected for the measured CNT emissivity of 0.825 (see Figure 1b). The average temperature of the roving was determined from a line scan along the centerline of the roving. Average temperatures of 50°C at 100 mA, 130°C at 200 mA, 223°C at 300 mA, and 330°C at 400 mA are observed. At an applied current above 400 mA (a current density of ~7.4 x 10^6 A/m^2), samples were not consistently stable and could undergo failure over time. Under vacuum, it is expected that the roving reaches somewhat higher temperature than those measured here, due to the lack of convective cooling. The decomposition of the $Cu(tBAOAC)_2$ precursor is reported at 225°C,[30] therefore, electrical bias conditions between 200 - 300 mA are expected to provide peak temperatures sufficient to cause deposition of the precursor to copper metal.

The effects of the electrical bias applied to the CNT roving during CVD are evaluated based upon the mass deposited and the nanoscale morphology analyzed via scanning electron microscopy (SEM). A scanning electron micrograph of the as-received CNT roving, prior to exposure to precursor is shown in Figure 2a. CNT bundles of various sizes (with diameters up to 100nm) are present, typically oriented along the axis of the CNT roving. An initial control sample with a heated mantle to evaporate the precursor, but no electrical bias through the roving during precursor exposure was prepared. The linear mass density of the roving increased by an

average of 68.4%, indicating the condensation of the $Cu(tBAOAC)_2$ precursor onto the cooler roving. The electron micrograph for the sample without bias, Figure 2b, exhibits unreacted precursor as a film on its surface, however, no nanoparticle formation. Strands of roving were subsequently biased at currents of 100 mA, 200 mA, 300 mA, and 400mA over the course of a one-hour CFH-CVD. At 100 mA, Figure 2c, irregularly-shaped nodules of incompletely decomposed precursor are observed at various locations across the surface of the roving. At 200 mA, sparse nanoscale spherules are evident at various locations across the surface of the sample, as seen in Figure 2d. At 300 mA (see Figure 2e), an increase in the number of particles is noted at locations in which they were observed. As Figure 2f shows, at 400 mA spherules are observed across the majority of the segments analyzed. Overall, between 200 mA and 400 mA for a one-hour deposition, the evolution from sparse collections of particles to more dense and uniform deposition of 10 – 40 nm particles is observed as the CNT roving's temperature exceeds the threshold current, with an average increase in linear density of 1.58 mg/m (14.85% of the hybrid mass). Studies into deposition time at a constant current of 300 mA reveal a saturation-type effect on the deposited mass in this CHF-CVD setup. In a half-hour deposition at 300 mA, an average mass increase of 8.42% is measured. Beyond this, all deposition times from 1 to 2 hours lead to comparable average deposited masses of 14-15% of the composite mass, as is evident from Figure S1. The saturation of the vapor in the reaction vessel may be self-limiting the deposition due to the gaseous decomposition byproducts[30] of $Cu(tBAOAC)_2$, preventing further evaporation of the precursor.

A sample biased at 400 mA with a one-hour CHF-CVD was used as an archetypal example for further chemical and physical analysis. Under backscatter electron (BSE) imaging (Figure S2), high contrast was observed between the deposited spherules and the underlying CNT matrix,

indicating a much higher Z element is present in the spherules. Energy-dispersive X-ray spectroscopy (EDX) confirms that the deposited spherules are copper, as is highlighted in Figure S3 (and in Figure S4 from a 300 mA deposition). Notably, the deposition yields a seeded roving with similar resistance (375 Ω/m) to a control roving sample exposed to similarly high current (386 Ω/m). This is attributed to the fact that the deposited Cu metal exists as discretized spherules rather than a continuous film, as has been observed in other studies of Cu-CNT composites.[24,25] Nonetheless, a focused ion beam milled (FIB) cross-section of this sample (Figure 3) confirms that the deposition is present throughout the thickness of the low-density roving. Combined with a copper overcoat, this may prove useful for connecting interior areas of the sample, providing additional conductive pathways beyond those that may be achieved through a metal overcoat alone.

For comparison with the standard CHF-CVD setup, an alternate approach was pursued to maintain the roving under no electrical bias in a "delayed filament heated CVD" (DFH-CVD) setup. In the DFH-CVD setup, electrical bias is only applied at the end of the run, after the precursor has been allowed to condense on the CNT roving. Due to the lack of gaseous thermal decomposition byproducts, an increased mass of $Cu(tBAOAC)_2$ is expected to condense upon the roving conductor, since the pressure within the flask should not rise above the threshold of $Cu(tBAOAC)_2$ vaporization during the deposition. Slightly higher deposited masses of 16.11% were obtained through the DFH-CVD method in a one-hour deposition followed by a 400 mA bias applied under 5% H_2/95% Ar. However, examinations of particle morphology reveal the nanoscale copper spherules noted under CHF-CVD (Figure 4a,b) have been replaced by larger microscale spheres of copper (Figure 4c,d) The change in particle size could be caused by the adhesion of the $Cu(tBAOAC)_2$ film to itself during decomposition. Since there is limited

adhesion between CNTs and metallic Cu,[26,31] the precursor may ripen into larger spheres rather than locally depositing as nanoparticles. Thus, it would appear advantageous to have consistent electrical bias applied throughout the deposition process, to ensure that hot spots on the CNT roving decompose the precursor locally.

While 400 mA was able to produce a uniform deposition along the roving, 300 mA is a more stable condition to evaluate whether site selectivity is possible during deposition. Thus, CFH-CVD was also performed with a 300 mA bias on a length of roving into which a knot had been tied (Figure 5a) to evaluate whether location-specific heating is a cause of preferential copper deposition from the vapor-phase precursor. Thermal imaging in air demonstrates that the presence of a knot in the CNT roving can generate a localized hot spot under bias, as shown in Figure 5b. Figure S5 establishes that the presence of hot spots can also be verified through incandescence at higher applied currents (≥450 mA) under vacuum. After the one-hour, 300 mA CFH-CVD, segments from a knotted piece of roving were characterized by SEM. Heavy amounts of deposited copper are observed at and immediately around the knots, as in Figure 5c. At the distance of ~1 cm away from the knots, the deposition appears much lighter, as in Figure 5d. Thus, the results indicate that metal is preferentially deposited with higher local temperature – a key potential advantage of this technology over nonspecific deposition methods such as electrodeposition or sputtering. Although the present focus demonstrates macro- to milli-scale control over depositions, closer modulation of the current may allow for the tuning of the deposition towards the nanoscale if individual CNT to CNT junctions are able to be selectively heated.

A copper overcoat was electrodeposited onto samples which had undergone CFH-CVD seeding pretreatment with a bias of 300 mA to produce finished electrical conductors. In recent

literature, metallic fractions of over 90% of the composite mass are common.[21,23,24,26,32] This is primarily due to the drastic difference between the densities of copper (8.96 g/cm^3) and carbon nanotubes (0.12 g/cm^3 for roving, towards 1 g/cm^3 or higher[13,33] in compressed wires[13,20,33,34]), which leads to composites that are around 50% copper by volume. In the present work, a variety of copper mass loadings were evaluated to provide a more complete understanding of the impact of the CVD pretreatment. All electroplating was carried out against copper anodes in a sandwich-cell configuration with a plating current of 12 A/g_{roving} for pre-determined times between one minute and one hour (Figure S6). Here, current is presented proportionally to the mass of the CNT roving (as A/g_{roving}) due to the porous, nanoscale network of the CNTs, which may lead to variation in local surface area along the length of the roving. Densification of the electroplated carbon nanotube wires was carried out in a rolling mill[33] to produce a ribbon-like conductor. Finally, the samples were annealed at 300°C for 3 hours under 5% H_2/95% Ar to reduce residual copper impurities.

Figure 6a plots the specific conductivity of samples with and without Cu(tBAOAC)$_2$ CFH-CVD as a pretreatment for electroplated CNT roving. The specific conductivity is defined as the bulk electrical conductivity normalized to sample density and provides a direct comparison of the gains made through metal incorporation and finishing.[1,10] The specific conductivity value relies on measurements of resistance per length and mass per length, thus avoiding the need to measure the cross-sectional area of each sample. The equation is given by:

$$\sigma_{sp} = \frac{\sigma}{D} = \frac{\frac{L}{RA}}{\frac{M}{LA}} = \frac{L^2}{RM}$$

where σ_{sp} is the specific conductivity, σ is the conductivity, D is the sample density, L is the length of the conductor, R is the resistance, A is the cross-sectional area, and M is the mass.[1] The independence from cross-sectional area accounts for any variations in density between lengths of

roving, and gains made through densification and annealing can be attributed to decreases in the linear resistance of the sample. Room temperature specific conductivity values in Figure 6a are presented after electroplating, after densification through calendaring, and after annealing. Below 60% mass loading, decreases in the samples' resistance were offset by increases in sample mass, leading to neutral (for CVD seeded) or negative (for non-seeed) changes in specific conductivity. While decreases in resistance per length are observed (156 Ω/m at 54.9% Cu for CVD pretreated after annealing compared to 368 Ω/m for 61.2% Cu with no pretreatment after annealing), the small volume fraction of the copper overcoat is likely unable to produce a strong electrical percolation network throughout the CNT roving. Between 54.9% w/w Cu and 78.9% w/w Cu, substantial increases are observed in the specific conductivity of the CVD pretreated samples. Specific conductivity values as high as 5632 $S \cdot m^2/kg$ (with resistance per length of 1.14 Ω/m) are attained for a sample with 94.2% copper mass. However, without CVD pretreatment, there is no substantial change in the specific conductivity of the electroplated samples. At 94.1% Cu, electroplated CNT roving has resistance per length reduced to 26.0 Ω/m, yet only reaches a specific conductivity of 218 $S \cdot m^2/kg$, substantially lower than the 407 $S \cdot m^2/kg$ starting specific conductivity of the roving. This indicates much improved utilization of the electrodeposited copper mass through the selective deposition of Cu from the $Cu(tBAOAC)_2$ precursor.

A measurement of the temperature coefficient of resistance (TCR) of the $Cu(tBAOAC)_2$ seeded Cu-CNT hybrid conductors were taken under vacuum over the range of 300K to 600K. As the mass fraction of Cu increases, the TCR for the Cu-CNT hybrid conductors, measured with respect to 300K, appears to follow a much more positive (metal-like) trend than the as-received CNT roving (which has a TCR of 2.18×10^{-4} K^{-1}), as displayed in Figure 7a**Figure 6**. However, even at 94.2% w/w Cu the $Cu(tBAOAC)_2$ seeded and electroplated sample's average

measured TCR_{300K} of 3.53 x 10^{-3} K^{-1} is still lower than the standard 3.83 x 10^{-3} K^{-1} for annealed copper.[6] This lower TCR leads to less relative loss in conductivity at elevated temperatures.

One proposed advantage of the Cu-CNT hybrid conductor for applications at elevated temperatures is the beneficial combination of high specific conductivity at a lower TCR. Consider a limiting case in which the Cu and CNT fractions of a conductor operate as discrete, non-interacting layers. Each layer could be envisioned as carrying a portion of the current, and thus on the bulk scale the system could be modeled as parallel resistors. In such a case, the expected specific conductivity and TCR may be determined based on the mass fraction of Cu and CNTs in such a layered structure with the intrinsic values for the pure materials (see Figure S10 for the equations). The predicted value relationship for TCR vs. room temperature specific conductivity over the continuum from 100% Cu conductor to 100% CNT roving conductor is shown in Figure 7b. The measured values obtained for the finished $Cu(tBAOAC)_2$ seeded and electroplated samples are also shown on this graph. Between 88.9% and 94.2% w/w Cu, the $Cu(tBAOAC)_2$ seeded and electroplated hybrids "cross-over" the threshold line representing the parallel resistors model. Therefore, the 94.2% w/w CNT-Cu hybrid represents a better combination of TCR and specific conductivity than would be expected from a simple combination of its constituent materials. Thus, there is evidence that the combination of CNTs and Cu in the material presented exhibit properties of a true hybrid rather than a layered composite.

Mechanical properties for a 94.2% w/w Cu-CNT hybrid are presented in Figure S7. The tensile strength of 92 MPa and Young's modulus of 11.6 GPa fall in between values obtained from the as-received roving (58 MPa tensile strength, 2.75 GPa Young's modulus) and a 12 μm copper foil with similar linear mass density and width to the sample (225 MPa tensile strength,

40.9 GPa Young's modulus). Figure S8 demonstrates that the annealed 94.2% w/w Cu-CNT hybrid exhibits less than 3% increase in resistance over 1000 bend cycles, consistent with properties for 12 μm Cu foil.

The conductivity of the 94.2% w/w Cu-CNT hybrid sample was determined by measuring the width of the sample via optical microscopy and thickness via SEM (Figure S8). The cross sectional area was determined to be 3.04×10^{-8} m^2 at the cut section of the Cu-CNT hybrid, resulting in a room temperature electrical conductivity of 2.81×10^{7} S/m. Figure 8 compares the present work to other recently published Cu-CNT hybrid conductors – where the electrical conductivity result from the combination of CFH-CVD with aqueous electrodeposition is among the highest reported at this mass loading of copper. This is particularly notable in that a low density (0.12 g/cm^3) (and high void space) starting material with an electrical conductivity at room temperature of only 4.94 x 10^4 S/m was enhanced by 569 times the original electrical conductivity. Thus, the CVD and electroplating technique is expected to be adaptable to various quality CNT conductor starting materials. Furthermore, the measured composite density of 5.14 g/cm^3 is only 61.4% of the calculated value for a sample consisting of 5.8% CNT roving and 94.2% Cu by mass based on a rule-of-mixtures. Optimizing this conductor density through improved densification techniques may yield further gains even without major process modifications. Overall, the CVD process is a demonstrated technique to selectively deposit nanometal Cu seeds onto CNT roving for enhanced electroplating utilization leading to hybrid structures with high electrical conductivity.

Conclusions:

The site-selective CVD of nanometal copper from $Cu(tBAOAC)_2$ has been demonstrated as an effective pretreatment method for the production of high conductivity copper-CNT hybrid

conductors. Using Joule heating of a CNT conductor to drive the CVD process is a robust, tunable, and scalable method towards more efficient use of metal mass within hybrid bulk conductors. The combination of CVD with conventional electroplating techniques outperforms standard electroplating over a wide range of mass loadings. Copper-CNT hybrids with room temperature specific conductivities of 5632 $S \cdot m^2/kg$ and electrical conductivities of 2.81 x 10^7 S/m have been demonstrated with this approach. These results represent increases of 13.8X and 569X the as-received CNT roving's specific conductivity (407 $S \cdot m^2/kg$) and conductivity (4.94 x 10^4 S/m), respectively. Further tuning of the nanometal seed mass and distribution through adjustment of the deposition parameters may produce even better utilization of added Cu mass. The CVD process also can be adapted to a wide variety of precursors using various metals, and presents a significant opportunity for advancing the field of metal-CNT hybrid conductors. Certain metals, such as platinum, palladium, or nickel which have improved bonding interactions towards carbon nanotubes may prove to be even better candidates for such vapor deposited seeds. The utility of this method lies in the fact that the CVD-produced seeds are uniquely deposited in localized regions due to the temperature differences (from the localized resistance) which contrasts with previous electroplating work where seed deposition is non-specific. While this paper has demonstrated macro- to micro-scale control over depositions, further selectivity towards the nanoscale could potentially be obtained through the application of a pulsed current through the CNT substrate which would modify the localized heating. Additionally, the process timescale for CVD seeding can be minutes to hours rather than hours to days for previous electroplating seed procedures. Thus, the described approach represents an emerging strategy to fabricate various metal-CNT hybrid conductors with enhanced temperate-dependent electrical properties for applications like rotating machinery and electric motors.

Experimental:

The carbon nanotube conductor used in this study is Miralon® roving from Nanocomp Technologies Inc. The roving is ribbon-like in form, with approximate dimensions of 30 μm x 1.8 mm and an average mass per length of 8.66 mg/m. It consists of a loose network of CNT bundles with an average density of 0.12 g/cm^3, and can be produced on the kilometer scale. The CNT roving is vacuum dried in an oven at 100°C for at least one hour prior to CVD or characterization. Thermogravimetric analysis and a Raman spectrum of this starting material are presented in Figure S12. The TGA establishes decomposition temperatures higher than 600°C and 15.4% residual ash. Raman data demonstrates a D/G ratio of 0.059, a G'/G ratio of 0.230, and a G'/D ratio of 3.89, indicating high purity CNTs in accordance with previous work.[35]

The chemical vapor deposition (CVD) setup is based on a three-neck flask. Through the two opposite necks of the flask, a copper electrical lead crimped to a flat clip is passed through a rubber septum. The roving is clamped between the clips, suspending the material across the center portion of the flask. A 10-12 cm length of roving is chosen so that it remains suspended and does not contact any of the walls of the flask. Under an inert argon atmosphere in a glovebox, $Cu(tBAOAC)_2$ precursor (CAS #23670-45-3, 99%, Strem) is added to the bottom of the flask through the third neck. A hose-barb adapter with a stopcock is then used to seal the center neck of the flask. The flask is removed from the glovebox, and the hose-barb is then hooked up to a Schlenk line which can provide either a vacuum or 5% H_2/95% (mol/mol) Ar atmosphere. The flask is placed in a heating mantle, which will be used to evaporate the precursor, and wrapped in glass wool for insulation.

In the standard continuous filament heating CVD (CFH-CVD) process, the flask is sequentially evacuated under vacuum then purged with 5% H_2/95% Ar four times. The flask is

then evacuated for at least ten minutes prior to the deposition to reach a pressure of 166 mBar, after which the stopcock is closed. A constant electrical bias of 100, 200, 300 or 400 mA is applied to the roving to induce Joule heating, and the flask is heated using a heating mantle to a set temperature of 155°C over the period of 10 minutes to begin the evaporation of the $Cu(tBAOAC)_2$. As the flask heats, vacuum is applied every 20°C to ensure the low pressure is maintained within the flask until the deposition starts. The $Cu(tBAOAC)_2$ precursor typically evaporates from a liquid phase (melting at a mantle temperature of ~150°C) rather than sublimating from its solid state. The CVD setup is maintained at the set temperature for a period between 0.5 and 2.0 hours to allow the deposition to occur. After the deposition has occurred, the heating mantle is removed, and the flask is purged with 5% H_2/95% Ar. After allowing the flask to cool for five minutes, the electrical bias is removed and the vapor-deposited roving is removed for electrical testing.

For the delayed filament heated CVD (DFH-CVD) method, no electrical bias is applied to the CNT roving during the one-hour deposition process. However, the precursor is still heated to 155°C, allowing for the condensation (without decomposition) of the precursor onto the relatively cooler roving. After the condensation has occurred, the flask is purged with 5% H_2 /95% Ar. A current of 400 mA is then applied to the roving to induce Joule heating and cause the decomposition of the precursor.

The Cu electroplating of both $Cu(tBAOAC)_2$-deposited and as-received CNT roving used a sandwich-style configuration (see Figure S6), where the sample was inserted within a folded piece of Whatman 42 filter paper to act as a separator. A piece of copper foil was wrapped around the filter paper to act as a counter electrode. This entire setup was sandwiched between two glass slides, and secured with Kapton tape to provide compression and ensure constant

distance between the CNT roving working electrode and copper counter electrode. The electrochemical cell was then submerged into a bath of acid copper electroplating solution (Transene). Electroplating was carried out under constant supplied current from an Arbin BT2000 battery tester. A constant cathodic current of 12 $A/g_{CNT\ roving}$ was applied over deposition times ranging from one minute to one hour (depending on the mass loading targeted). After electroplating, samples were rinsed with deionized water, and allowed to dry for 1 hour at 100°C under vacuum. Samples were then compressed in a rolling mill to improve electrical contact between the CNTs and deposited copper particles. The Cu-CNT hybrids were sandwiched between two 3 cm wide pieces of 18 μm thick copper foil. An initial gap size of 40 μm was chosen. Twenty passes were made through the rolling mill, reducing the gap by 1 μm every other pass. Finally, samples were annealed under 5% H_2/95% Ar gas at 300°C for 3 hours to reduce any remaining copper oxides and ensure good electrical contact between copper particles.

The samples were massed before and after the CVD and electroplating depositions using a Mettler Toledo XP-2U microbalance, and their lengths were measured using high-precision calipers. Electrical resistance was measured using a four-point probe connected to a National Instruments NI PXI-5652 source/measure unit and an NI PXI-4071 digital multimeter at room temperature (~20 °C) through a current-potential sweep. The temperature coefficient of resistance (TCR) was measured using a four-point probe setup within a Janis cryostat connected to a National Instruments NI PXI-4110 Programmable Power Supply and an NI PXI-4072 digital multimeter through a current-potential sweep. Resistance was measured at 10^{-6} mBar every 5 K over the range of 300 K to 600 K. Two cycles of temperature were measured and data from the second cycle is presented to minimize effects of temperature annealing through the first cycle.

The TCR was determined from the average slope of the resistance relative to 300K. A FLIR A35 IR Temperature Sensor was used to obtain thermal images of the CNT roving as a function of electrical bias. An emissivity correction of 0.825 was determined through ASTM E1933 for the CNT roving. Sample surface morphology was evaluated via a Hitachi S900 SEM equipped with an immersion lens and backscatter electron detector Secondary electron images were taken at 2 keV and backscatter electron images were taken at 10 keV. A Tescan Mira3 SEM equipped with a Bruker energy dispersive x-ray (EDX) spectrometer was used for elemental analysis of the sample surfaces. For cross-sectional imaging, the FIB milling, imaging and EDS were performed in a FEI scanning electron microscope (SEM)/Ga liquid metal ion source (LMIS) dual-beam tool, equipped with an Oxford Instruments X-Max 80 mm EDS x-ray detector. A CNT wire, mounted on a 45° Al stub and tilted 7° to align its surface normal with the FIB axis, was FIB cross-sectioned in three steps. A 30 keV Ga ion beam at 19 nA was used for the initial cut. Clean-up cuts were performed with an 8 keV Ga ion beam at 2.8 nA. The lower energy and ion beam current of the clean-up cuts helped to reduce damage of adjacent features and reduced the concentration of Ga near the surface. EDS mapping was performed using a 20 keV electron beam rastered over a region 2µm x 12 µm region at a tilt angle of 30° yielding an incident angle of 75°.

FIGURES

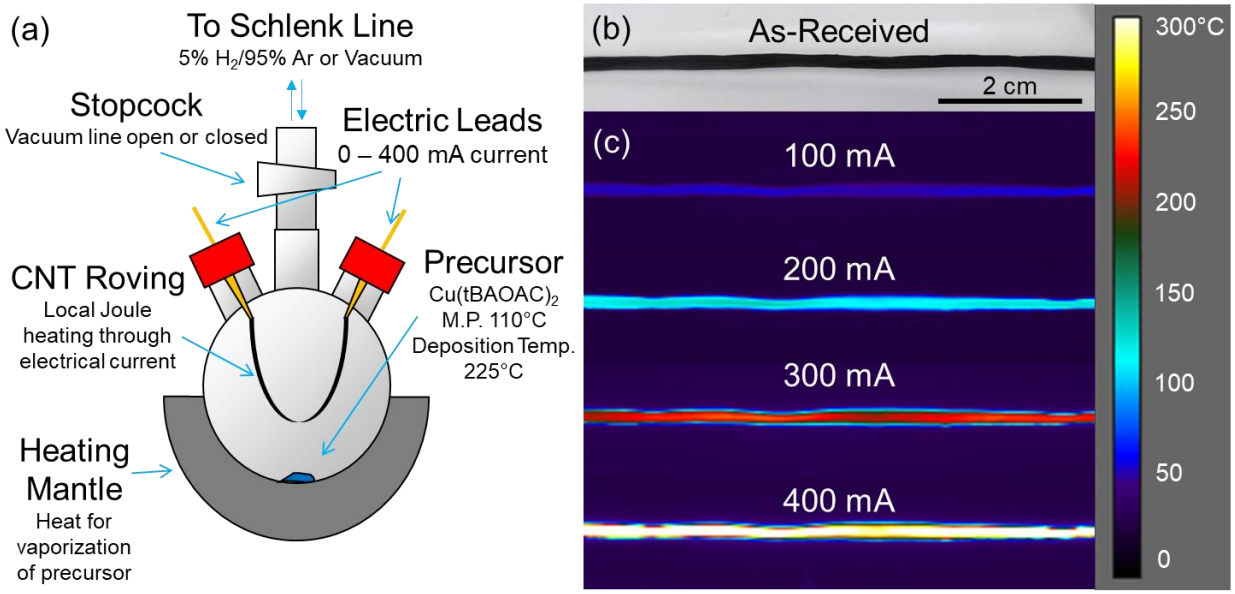

Figure 1. (a) The experimental setup utilized for the chemical vapor deposition, illustrating the various process controls that may be modified. (b) Optical image of CNT roving. (c) Thermal images of CNT roving biased under various currents in air, exhibiting a direct relationship between temperature and current.

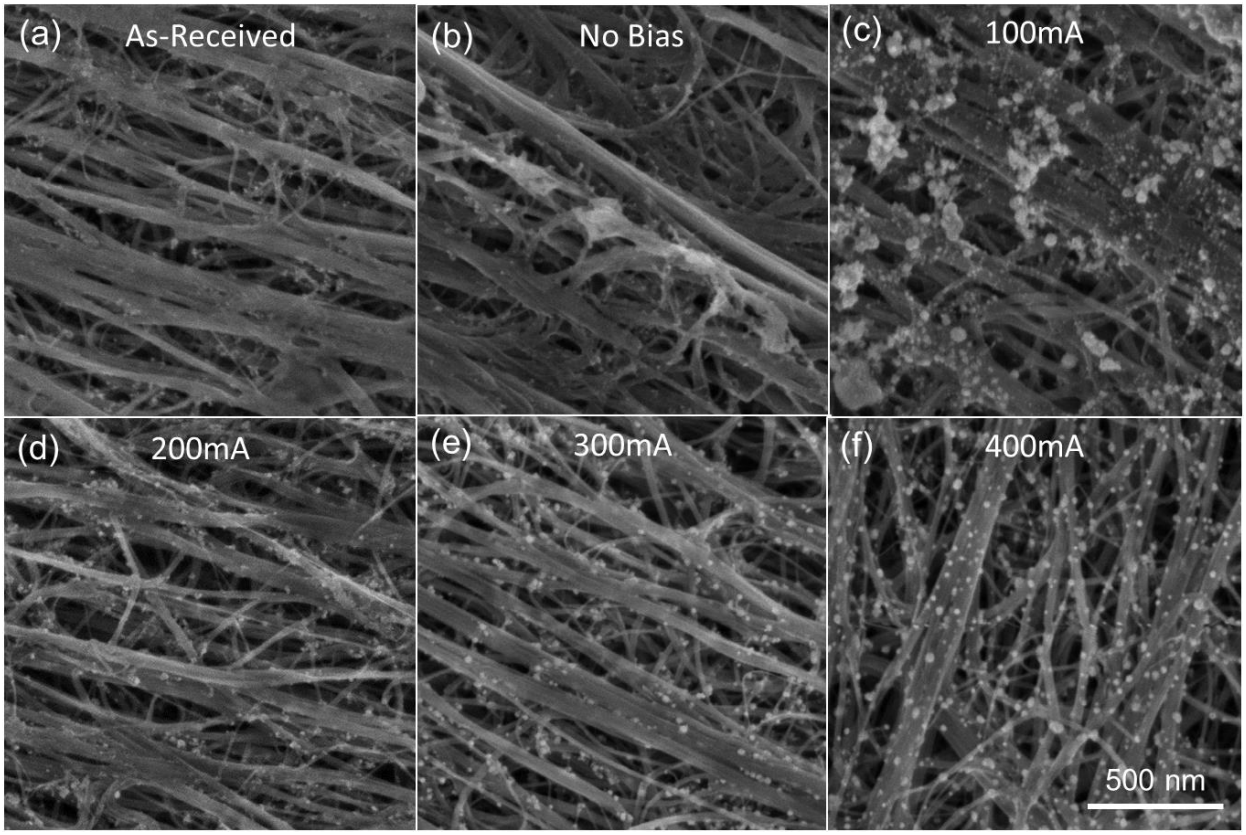

Figure 2. Secondary electron images of (a) as-received roving and roving after CFH-CVD (b) with no electrical bias, and at (c) 100 mA, (d) 200 mA, (e) 300 mA, and (f) 400 mA bias. Segments were taken for SEM analysis at least 1 cm from the end of the roving to minimize effects from conductive cooling through the electrical leads.

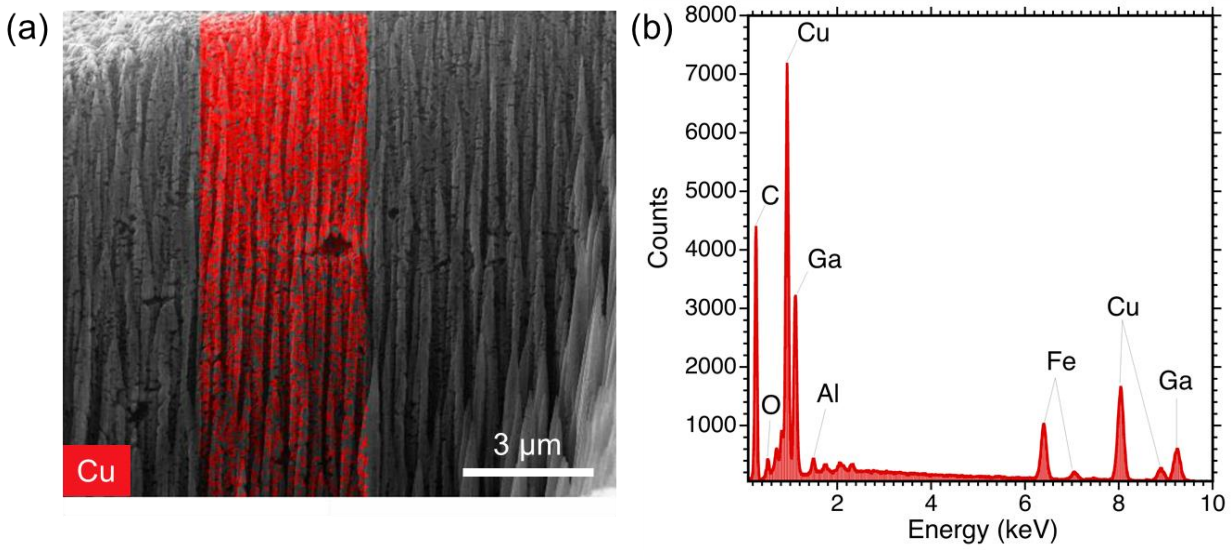

Figure 3. (a) EDX scan of the cross-section of the composite revealed by gallium FIB milling. Sample surface is visible at the top left of the image. Copper signal strength overlaid in red, demonstrating penetration of deposited copper towards the center of the 30 µm thick roving. (b) Histogram of signal frequency counts, demonstrating the prominence of the copper signal in the analyzed region.

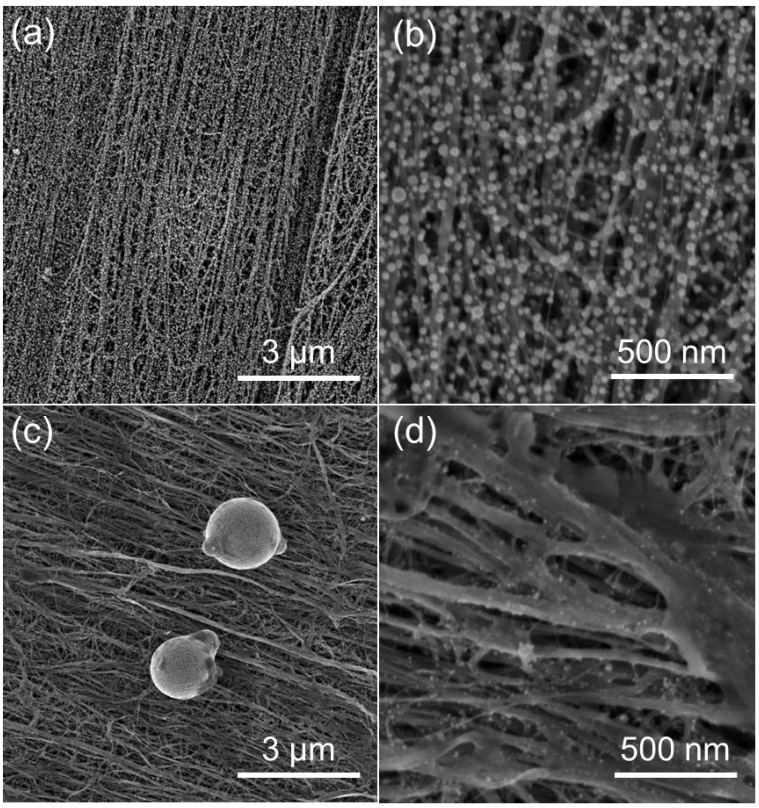

Figure 4. (a) Low and (b) high magnification images of a 400 mA CHF-CVD\. (c) Low and (d) high magnification images of a DFH-CVD with 400 mA bias at the end of the test.

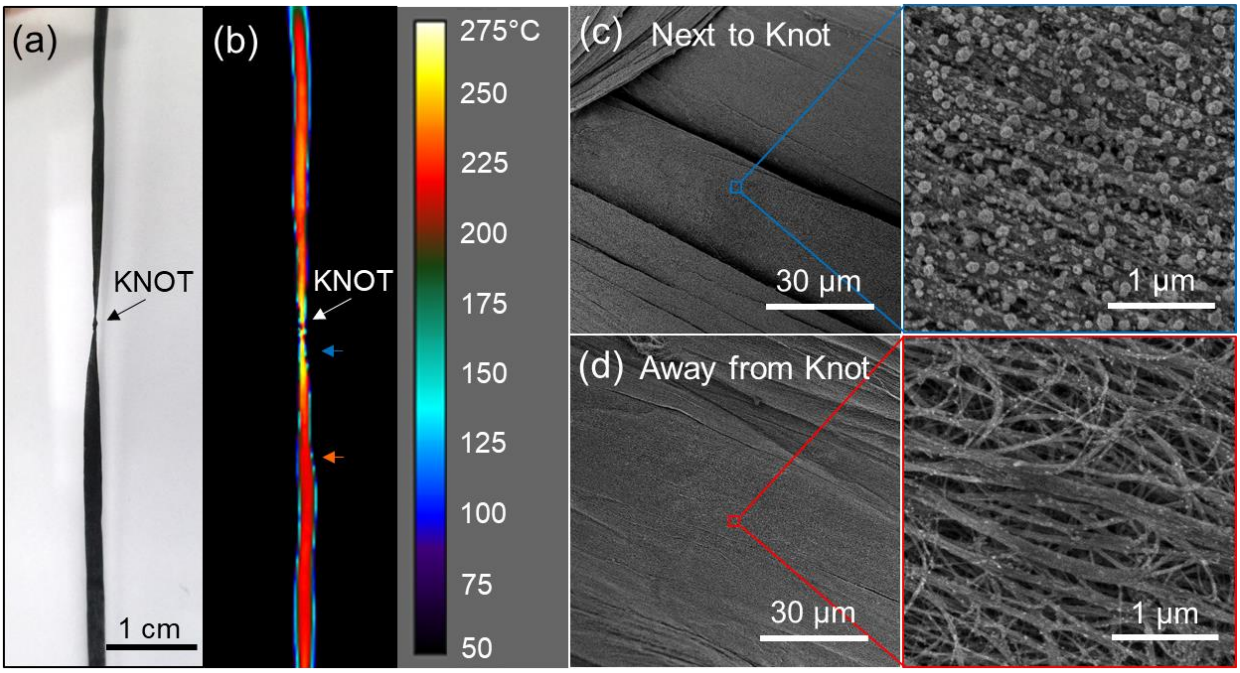

Figure 5. A knot tied in the roving (a) is able to generate a hot spot in neighboring regions, here demonstrated through thermal images (b) of a 300 mA bias in air. (c) SEM images of the region next to a knot after a 300 mA deposition. The knot is visible in the upper left of the image. (d) SEM images of a region ~1 cm away from the knot.

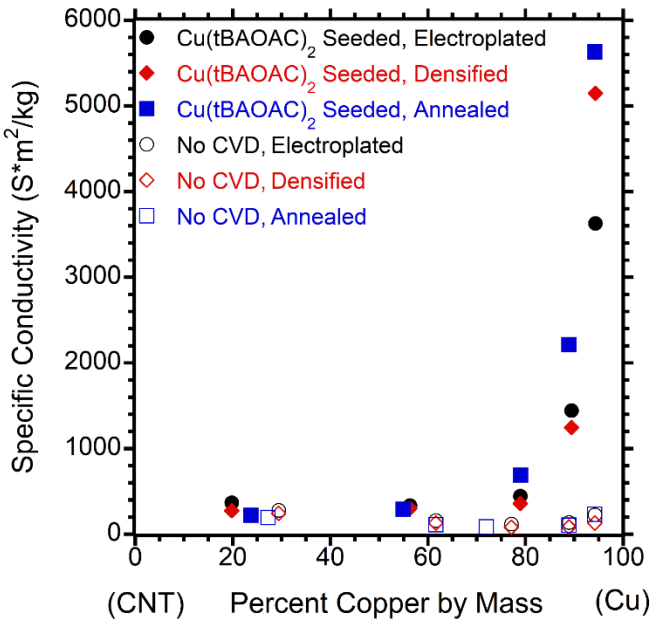

Figure 6. Specific conductivity of electroplated Cu-CNT hybrids with and without Cu seeding from $Cu(tBAOAC)_2$ plotted against total deposited Cu mass.

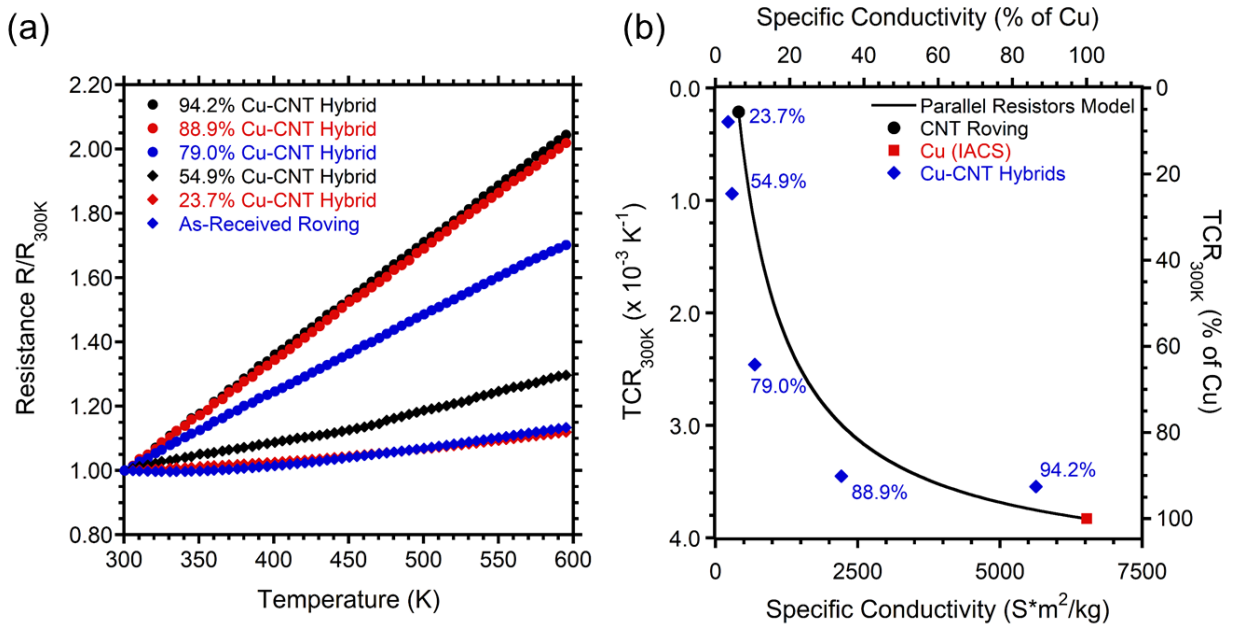

Figure 7. (a) Temperature dependent electrical resistance measurements (relative to 300K) under vacuum for each of the finished Cu-CNT hybrid conductors and the as-received CNT roving. The temperature coefficient of resistance (TCR) is determined from the average slope of resistance relative to 300 K. (b) Plot of the TCR and specific conductivity of Cu-CNT hybrid conductors compared to copper, CNT roving, and calculated combinations of the two materials based on the parallel resistors model.

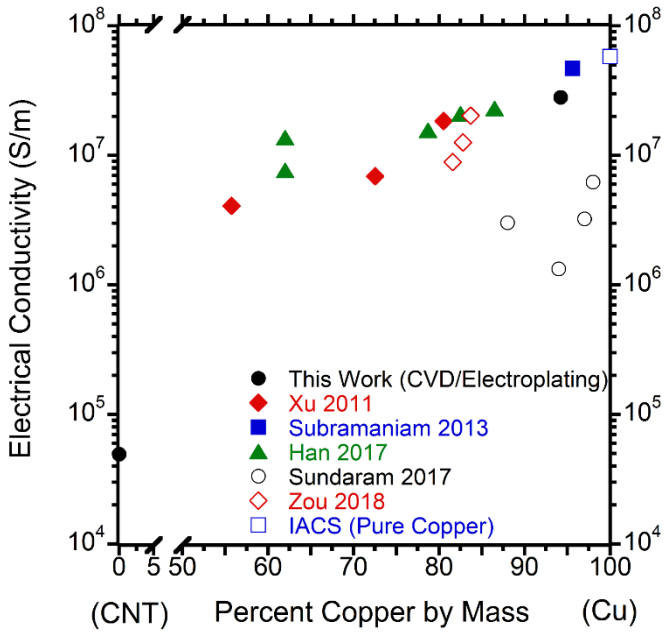

Figure 8. Room temperature conductivity of a 94.2% Cu composite produced through nanometal deposition of $Cu(tBAOAC)_2$ followed by copper electrodeposition, compared with other recent literature results: Xu 2011,[36] Subramaniam 2013,[21] Han 2017,[26] Sundaram 2017,[24] Zou 2018.[23] It is important to note that while some of the literature samples contain small mass fractions of other metals (e.g. Ni),[26] Cu is the majority metal within every composite.

ASSOCIATED CONTENT

Supplemental Figures (.docx)

AUTHOR INFORMATION

Corresponding Author

*brian.landi@rit.edu

Author Contributions

The manuscript was written through contributions of all authors. All authors have given approval to the final version of the manuscript.

Funding Sources

Department of Energy Grant #DE-EE0007863

ACKNOWLEDGMENT

The authors would like to thank Dr. Ivan Puchades, Dr. Reginald E. Rogers, and Dr. Stephen M. Ubnoske for helpful discussions. The authors acknowledge funding from the Advanced Manufacturing Office of the Office of Energy Efficiency and Renewable Energy of the U.S. Department of Energy under grant DE-EE0007863. The contents of this document should not be construed as asserting or implying U.S. Government authentication of information or endorsement of the authors' views.

ABBREVIATIONS

CFH-CVD, continuous filament heating chemical vapor deposition; CNT, carbon nanotube; $Cu(tBAOAC)_2$, bis(t-butylacetoacetato) copper (II); CVD, chemical vapor deposition; EDX,

energy dispersive x-ray spectroscopy; FIB, focused ion beam; DFH-CVD, delayed filament heating chemical vapor deposition; NICCs, nanometal interconnection of carbon conductors; SEM, scanning electron microscopy; TCR, temperature coefficient of resistance

REFERENCES

(1) Bucossi, A. R.; Cress, C. D.; Schauerman, C. M.; Rossi, J. E.; Puchades, I.; Landi, B. J. Enhanced Electrical Conductivity in Extruded Single-Wall Carbon Nanotube Wires from Modified Coagulation Parameters and Mechanical Processing. *ACS Appl. Mater. Interfaces* **2015**, *7*, 27299–27305.

(2) Jarosz, P.; Schauerman, C.; Alvarenga, J.; Moses, B.; Mastrangelo, T.; Raffaelle, R.; Ridgley, R.; Landi, B. Carbon Nanotube Wires and Cables: Near-Term Applications and Future Perspectives. *Nanoscale* **2011**, *3*, 4542–4553.

(3) Liu, K.; Sun, Y.; Zhou, R.; Zhu, H.; Wang, J.; Liu, L.; Fan, S.; Jiang, K. Carbon Nanotube Yarns with High Tensile Strength Made by a Twisting and Shrinking Method. *Nanotechnology* **2010**, *21*, 045708.

(4) Behabtu, N.; Young, C. C.; Tsentalovich, D. E.; Kleinerman, O.; Wang, X.; Ma, A. W. K.; Bengio, E. A.; Ter Waarbeek, R. F.; De Jong, J. J.; Hoogerwerf, R. E.; Fairchild S. B.; Ferguson J. B.; Maruyama, B.; Kono, J.; Talmon, Y.; Cohen, Y.; Otto, M. J.; Pasquali, M. Strong, Light, Multifunctional Fibers of Carbon Nanotubes with Ultrahigh Conductivity. *Science.* **2013**, *339*, 182–186.

(5) Lekawa-Raus, A.; Walczak, K.; Kozlowski, G.; Wozniak, M.; Hopkins, S. C.; Koziol, K. K. Resistance-Temperature Dependence in Carbon Nanotube Fibres. *Carbon* **2015**, *84*, 118–123.

(6) National Bureau of Standards. *Copper Wire Tables*, 3rd ed.; Stratton, S. W., Ed.; Washington, D.C., 1914.

(7) Buldum, A.; Lu, J. P. Contact Resistance between Carbon Nanotubes. *Phys. Rev. B* **2001**, *63*, 161403.

(8) Garrett, M. P.; Ivanov, I. N.; Gerhardt, R. A.; Puretzky, A. A.; Geohegan, D. B. Separation of Junction and Bundle Resistance in Single Wall Carbon Nanotube Percolation Networks by Impedance Spectroscopy. *Appl. Phys. Lett.* **2010**, *97*, 163105.

(9) Lee, J.; Stein, I. Y.; Devoe, M. E.; Lewis, D. J.; Lachman, N.; Kessler, S. S.; Buschhorn, S. T.; Wardle, B. L. Impact of Carbon Nanotube Length on Electron Transport in Aligned Carbon Nanotube Networks. *Appl. Phys. Lett.* **2015**, *106*, 053110.

(10) Lekawa-Raus, A.; Patmore, J.; Kurzepa, L.; Bulmer, J.; Koziol, K. Electrical Properties of Carbon Nanotube Based Fibers and Their Future Use in Electrical Wiring. *Adv. Funct. Mater.* **2014**, *24*, 3661–3682.

(11) Davis, V. A.; Parra-vasquez, A. N. G.; Green, M. J.; Rai, P. K.; Behabtu, N.; Prieto, V.; Booker, R. D.; Schmidt, J.; Kesselman, E.; Zhou, W.; Fan, H.; Adams, W. W.; Hauge, R. H.; Fischer, J. E.; Cohen, Y.; Talmon, Y.; Smalley, R. E.; Pasquali, M. True Solutions of Single-Walled Carbon Nanotubes for Assembly into Macroscopic Materials. *Nat. Nanotechnol.* **2009**, *4*, 830–834.

(12) Headrick, R. J.; Tsentalovich, D. E.; Berdegué, J.; Bengio, E. A.; Liberman, L.; Kleinerman, O.; Lucas, M. S.; Talmon, Y.; Pasquali, M. Structure-Property Relations in Carbon Nanotube Fibers by Downscaling Solution Processing. *Adv. Mater.* **2018**,

1704482, 1–8.

(13) Downes, R. D.; Hao, A.; Park, J. G.; Su, Y. F.; Liang, R.; Jensen, B. D.; Siochi, E. J.; Wise, K. E. Geometrically Constrained Self-Assembly and Crystal Packing of Flattened and Aligned Carbon Nanotubes. *Carbon* **2015**, *93*, 953–966.

(14) Alvarenga, J.; Jarosz, P. R.; Schauerman, C. M.; Moses, B. T.; Landi, B. J.; Cress, C. D.; Raffaelle, R. P. High Conductivity Carbon Nanotube Wires from Radial Densification and Ionic Doping. *Appl. Phys. Lett.* **2010**, *97*, 182106.

(15) Zhao, Y.; Wei, J.; Vajtai, R.; Ajayan, P. M.; Barrera, E. V. Iodine Doped Carbon Nanotube Cables Exceeding Specific Electrical Conductivity of Metals. *Sci. Rep.* **2011**, *1*, 83.

(16) Janas, D.; Milowska, K. Z.; Bristowe, P. D.; Koziol, K. K. K. Improving the Electrical Properties of Carbon Nanotubes with Interhalogen Compounds. *Nanoscale* **2017**, *9*, 3212–3221.

(17) Li, S.; Zhang, X.; Zhao, J.; Meng, F.; Xu, G.; Yong, Z.; Jia, J.; Zhang, Z.; Li, Q. Enhancement of Carbon Nanotube Fibres Using Different Solvents and Polymers. *Compos. Sci. Technol.* **2012**, *72*, 1402–1407.

(18) Liu, P.; Hu, D. C. M.; Tran, T. Q.; Jewell, D.; Duong, H. M. Electrical Property Enhancement of Carbon Nanotube Fibers from Post Treatments. *Colloids Surfaces A Physicochem. Eng. Asp.* **2016**, *509*, 384–389.

(19) Cress, C. D.; Ganter, M. J.; Schauerman, C. M.; Soule, K.; Rossi, J. E.; Lawlor, C. C.; Puchades, I.; Ubnoske, S. M.; Bucossi, A. R.; Landi, B. J. Carbon Nanotube Wires with

Continuous Current Rating Exceeding 20 Amperes. *J. Appl. Phys.* **2017**, *122*, 025101.

(20) Di, J.; Fang, S.; Moura, F. A.; Galvão, D. S.; Bykova, J.; Aliev, A.; de Andrade, M. J.; Lepró, X.; Li, N.; Haines, C.; Ovalle-Robles, R.; Qian, D.; Baughman, R. H. Strong, Twist-Stable Carbon Nanotube Yarns and Muscles by Tension Annealing at Extreme Temperatures. *Adv. Mater.* **2016**, 6598–6605.

(21) Subramaniam, C.; Yamada, T.; Kobashi, K.; Sekiguchi, A.; Futaba, D. N.; Yumura, M.; Hata, K. One Hundred Fold Increase in Current Carrying Capacity in a Carbon Nanotube–copper Composite. *Nat. Commun.* **2013**, *4*, 1–7.

(22) Subramaniam, C.; Sekiguchi, A.; Yamada, T.; Futaba, D. N.; Hata, K. Nano-Scale, Planar and Multi-Tiered Current Pathways from a Carbon Nanotube–copper Composite with High Conductivity, Ampacity and Stability. *Nanoscale* **2016**, *8*, 3888–3894.

(23) Zou, J.; Liu, D.; Zhao, J.; Hou, L.; Liu, T.; Zhang, X.; Zhao, Y.; Zhu, Y. T.; Li, Q. Ni Nanobuffer Layer Provides Light-Weight CNT/Cu Fibers with Superior Robustness, Conductivity, and Ampacity. *ACS Appl. Mater. Interfaces* **2018**, *10*, 8197–8204.

(24) Sundaram, R.; Yamada, T.; Hata, K.; Sekiguchi, A. Electrical Performance of Lightweight CNT-Cu Composite Wires Impacted by Surface and Internal Cu Spatial Distribution. *Sci. Rep.* **2017**, *7*, 9267.

(25) Janas, D.; Koziol, K. K. K. The Influence of Metal Nanoparticles on Electrical Properties of Carbon Nanotubes. *Appl. Surf. Sci.* **2016**, *376*, 74–78.

(26) Han, B.; Guo, E.; Xue, X.; Zhao, Z.; Luo, L.; Qu, H.; Niu, T.; Xu, Y.; Hou, H. Fabrication and Densification of High Performance Carbon Nanotube/Copper Composite Fibers.

Carbon **2017**, *123*, 593–604.

(27) Cox, N. D.; Rape, A.; Pham, M.; Rossi, J. E.; Bucossi, A. R.; Landi, B. J. Free-Standing Silver/Carbon Nanotube Metal Matrix Composite Thin Films. *J. Mater. Sci.* **2016**, *51*, 10935–10942.

(28) Sundaram, R.; Yamada, T.; Hata, K.; Sekiguchi, A. The Influence of Cu Electrodeposition Parameters on Fabricating Structurally Uniform CNT-Cu Composite Wires. *Mater. Today Commun.* **2017**, *13*, 119–125.

(29) Do, J. W.; Estrada, D.; Xie, X.; Chang, N. N.; Mallek, J.; Girolami, G. S.; Rogers, J. A.; Pop, E.; Lyding, J. W. Nanosoldering Carbon Nanotube Junctions by Local Chemical Vapor Deposition for Improved Device Performance. *Nano Lett.* **2013**, *13*, 5844–5850.

(30) Devi, A.; Goswami, J.; Lakshmi, R.; Shivashankar, S. a; Chandrasekaran, S.; Introduction, I. A Novel Cu(II) Chemical Vapor Deposition Precursor: Synthesis, Characterization, and Chemical Vapor Deposition. *J. Mater. Res.* **1998**, *13*, 687–692.

(31) Milowska, K. Z.; Ghorbani-Asl, M.; Burda, M.; Wolanicka, L.; Ćatić, N.; Bristowe, P. D.; Koziol, K. K. K. Breaking the Electrical Barrier between Copper and Carbon Nanotubes. *Nanoscale* **2017**, *9*, 8458–8469.

(32) Hannula, P. M.; Peltonen, A.; Aromaa, J.; Janas, D.; Lundström, M.; Wilson, B. P.; Koziol, K.; Forsén, O. Carbon Nanotube-Copper Composites by Electrodeposition on Carbon Nanotube Fibers. *Carbon* **2016**, *107*, 281–287.

(33) Wang, J. N.; Luo, X. G.; Wu, T.; Chen, Y. High-Strength Carbon Nanotube Fibre-like Ribbon with High Ductility and High Electrical Conductivity. *Nat. Commun.* **2014**, *5*,

3848.

(34) Han, B.; Guo, E.; Xue, X.; Zhao, Z.; Li, T.; Xu, Y.; Luo, L.; Hou, H. Enhancement of the Twisted Carbon Nanotube Fibers Properties by Drawing Processing and Acid Treatment. *Mater. Des.* **2018**, *143*, 238–247.

(35) DiLeo, R. a.; Landi, B. J.; Raffaelle, R. P. Purity Assessment of Multiwalled Carbon Nanotubes by Raman Spectroscopy. *J. Appl. Phys.* **2007**, *101*, 064307.

(36) Xu, G.; Zhao, J.; Li, S.; Zhang, X.; Yong, Z.; Li, Q. Continuous Electrodeposition for Lightweight, Highly Conducting and Strong Carbon Nanotube-Copper Composite Fibers. *Nanoscale* **2011**, *3*, 4215–4219.

TOC GRAPHIC